PNAS RESEARCH ARTICLE | DEVELOPMENTAL BIOLOGY

# Zscan4 mediates ubiquitination and degradation of the corepressor complex to promote chromatin accessibility in 2C-like cells

Jiao Yang[a,b,c,d,1], Jiameng Dan[c,d,1], Nannan Zhao[a,b,e], Linlin Liu[a,b], Huasong Wang[a,b], Qiangqiang Liu[a,b], Lingling Wang[a,b], Jie Li[a,b], Yiwei Wu[a,b], Feilong Chen[a,d], Weilun Fu[a], Fei Liu[a], Meiqi Lin[c,d], Weiyu Zhang[a], Fuquan Chen[a], Xinqi Liu[a,f], Xinyi Lu[a,g], Quan Chen[a,b], Xudong Wu[h], Yuyu Niu[c,d,2], Na Yang[a,2], Yushan Zhu[a,b,2], Jiafu Long[a,f,2], and Lin Liu[a,b,e,i,2]

Affiliations are included on p. 11.

Edited by Marisa Bartolomei, University of Pennsylvania Perelman School of Medicine, Philadelphia, PA; received April 15, 2024; accepted November 11, 2024

**Zygotic genome activation occurs in two-cell (2C) embryos, and a 2C-like state is also activated in sporadic (~1%) naïve embryonic stem cells in mice. Elevated chromatin accessibility is critical for the 2C-like state to occur, yet the underlying molecular mechanisms remain elusive. Zscan4 exhibits burst expression in 2C embryos and 2C-like cells. Here, we show that Zscan4 mediates chromatin remodeling to promote the chromatin accessibility for achieving the 2C-like state. Through coimmunoprecipitation/mass spectrometry, we identified that Zscan4 interacts with the corepressors Kap1/Trim28, Lsd1, and Hdac1, also with H3K9me3 modifiers Suv39h1/2, to transiently form a repressive chromatin complex. Then, Zscan4 mediates the degradation of these chromatin repressors by recruiting Trim25 as an E3 ligase, enabling the ubiquitination of Lsd1, Hdac1, and Suv39h1/2. Degradation of the chromatin repressors promotes the chromatin accessibility for activation of the 2C-like state. These findings reveal the molecular insights into the roles of Zscan4 in promoting full activation of the 2C-like state.-**

Zscan4 | chromatin accessibility | zygotic genome activation | 2C like state | ubiquitination

## Significance

Two-cell (2C) embryos and 2C-like cells (2CLCs) sporadically arising in mouse embryonic stem cells (mESCs) are associated with increased chromatin accessibility, ensuring the burst expression of transcripts that occur during zygotic genome activation (ZGA). Here, we demonstrate the pivotal roles of Zscan4 in promoting the chromatin accessibility in 2CLCs. By forming a transiently repressive chromatin complex with corepressors Kap1/Trim28, Lsd1, Hdac1, and Suv39h1/2, Zscan4 facilitates the ubiquitination and degradation of these repressors by recruiting the E3 ligase Trim25. The degradation of those corepressors facilitates the chromatin accessibility for activation of 2C-like genes in mESCs.

During early mammalian development, fertilization results in rapid and extensive chromatin remodeling as well as genome-wide DNA demethylation driven by maternally inherited components. This ensures the activation of new transcription from the zygotic genome, or zygotic genome activation (ZGA), during maternal-to-zygotic transition (MZT) (1–5). Recent advances revealed the PRD-like homeobox domain transcription factor oocyte specific homeobox (OBOX; OBOX1-OBOX8) and tetrapeptide repeat homeobox (TPRX; TPRX1, TPRX2, and TPRXL) as the key regulators for mouse and human ZGA, respectively (6, 7). ZGA occurs at the two-cell (2C) stage during early embryo development in mice and is accompanied by zygotic transcription associated with extensive epigenetic reprogramming including heterochromatin modification and dramatically increased chromatin accessibility (1, 3, 8–15). Heterochromatin changes take place during MZT, and the progressive acquisition of H3K9me3 landscapes in maternal and paternal chromosomes occurs around the time of zygote genome expression (1, 16). Moreover, the drastic reprogramming of H3K9me3-dependent heterochromatin upon fertilization removes H3K9me3 barriers from promoter regions, creating a less constrained epigenetic environment for subsequent ZGA (13, 17).

Consistently, early mouse embryos possess broad regions of open chromatin that are narrowed down to mark promoters by the time of the major wave of ZGA occurring (8, 10, 18). Chromatin accessibility profiling revealed that defined regulatory regions and transcriptional activation are established concomitantly (9, 10). Moreover, transcription of minor ZGA (such as *Zscan4*) and major ZGA is regulated by RNA polymerase II (Pol II) and open chromatin (14, 15). Like 2C embryos, 2C-like cells (2CLCs) which represent a small subpopulation of mouse embryonic stem cells (mESCs), exhibit an increase in global chromatin accessibility, particularly at 2C-like genes and endogenous retroviruses (*MERVLs*) (4, 19–21). Globally decondensed chromatin is associated with increased histone acetylation and higher chromatin mobility (21, 22). Also, increased histone acetylation is associated with gene activation during ZGA (5). However, the molecular mechanisms underlying the chromatin accessibility and elevated histone acetylation in the full activation of the 2C-like state remain elusive.

Notably, *Zscan4* is actively transcribed at minor ZGA right after zygotic cleavage (10). In addition, *Zscan4* and *MERVLs* that are specifically expressed in 2C embryos are activated in sporadic 2CLCs in mESC cultures (23–25). Zscan4 has been

Author contributions: J.Y., J.D., Y.N., N.Y., Y.Z., J. Long, and Lin Liu designed research; J.Y., J.D., H.W., Q.L., L.W., J. Li, Y.W., Feilong Chen, W.F., M.L., W.Z., and Fuquan Chen performed research; X. Liu, X. Lu, Q.C., X.W., Y.Z., and J. Long contributed new reagents/analytic tools; J.Y., J.D., N.Z., Linlin Liu, F.L., N.Y., and Lin Liu analyzed data; and J.Y., J.D., and Lin Liu wrote the paper.

The authors declare no competing interest.

This article is a PNAS Direct Submission.



[1]J.Y. and J.D. contributed equally to this work.

[2]To whom correspondence may be addressed. Email: niuyy@lpbr.cn, yangnanku@nankai.edu.cn, zhuys@nankai.edu.cn, jflong@nankai.edu.cn, or liulin@nankai.edu.cn.

This article contains supporting information online at https://www.pnas.org/lookup/suppl/doi:10.1073/pnas.2407490121/-/DCSupplemental.

Published December 20, 2024.

demonstrated to elongate telomeres in mESCs (23, 26, 27), and implicated in telomere lengthening in 2C embryos (28). Additionally, Zscan4 functions in DNA damage repair, as shown by binding to nucleosomes to protect fragile genomic regions from DNA damage and by increasing induction and quality of induced pluripotent stem cells (29, 30). Extensive research has revealed how Zscan4 is activated. Specifically, OBOX (7), Dux (20, 31, 32), Dppa2/4 (33–35), Dcaf11 (36), and retinoic acid (37) that promote 2C-like state transition in mESC cultures also activate *Zscan4* and *MERVLs* in early embryos. Excitingly, totipotent potential stem cells, totipotent-like stem cells, chemically induced totipotent stem cells, or totipotent blastomere-like cells resembling 2C stage embryos have been achieved from mESCs by chemical induction, and notably, the 2C marker gene *Zscan4* served as one of the key totipotent-related genes (38–42).

Here, we report critical functions of Zscan4 in chromatin remodeling by facilitating ubiquitination and degradation of corepressors to promote the chromatin accessibility for the 2C-like state.

## Results

**Dynamics of Zscan4 during Heterochromatin Decondensation in 2C Embryos.** It has been shown that *Zscan4* messenger RNA (mRNA) is specifically transcribed in 2C embryos during mouse preimplantation development (10, 25, 43). Zscan4 protein expression dynamics has not been examined at specific time points during 2C stage embryo development, and it remains unclear when the Zscan4 protein expression begins and reaches the highest level in the 2C mouse embryos. Accordingly, we examined the spatiotemporal dynamics of Zscan4 protein expression by immunofluorescence during mouse 2C embryo development. To precisely time Zscan4 protein expression at the 2C stage, we collected 2C embryos at more time points (every 3 to 4 h) post zygotic cleavage until entering the 4-cell stage. The entire period of the 2C embryo stage takes about 22 to 24 h, comparable to that of in vivo (10, 25). Zscan4 protein was expressed in the nuclei of majority of 2C embryos 6 to 7 h post zygotic cleavage, approximating 37 to 38 h after hCG injection (Fig. 1*A* and *SI Appendix*, Fig. S1). Zscan4 protein was expressed at the highest level 11 to 12 h post the cleavage in the nuclei of mid-2C stage embryos (Fig. 1*A*). Background staining seen on the cell membrane could be due to the Zscan4 polyclonal antibody available.

The dynamic changes of Zscan4 protein prompted us to look at what happened to the epigenetic regulation such as heterochromatin changes at the specific time points. The highest Zscan4 protein expression level was accompanied by a reduced H3K9me3 level, with fewer heterochromatin foci during the middle stage (12 h) in 2C embryos (Fig. 1 *B* and *C*). Consistently, a previous study has demonstrated that the enrichment of H3K9me3 at the *Zscan4* locus decreases to the lowest level in the 2C stage embryo, increases in the 4C stage embryo, and maintains at stable levels during the later preimplantation development, coinciding the highest Zscan4 protein level in mid-2C embryos. However, the non-2C-gene *Gnas* does not show this expression pattern and exhibits consistent high levels of H3K9me3 mark from 2C to blastocyst stage (13). H3K9me3 level was increased by 20 h, while the Zscan4 protein level was low. During the first 7 to 8 h after cleavage, the heterochromatin imaged using DAPI staining was not evenly distributed in the nucleus and more concentrated around the nucleolus. Hence, the elevated Zscan4 protein level precedes the major ZGA that takes place during the late 2C stage undergoing extensive transcription by RNA Pol II (14).

**Dynamics of Zscan4 and Heterochromatin Remodeling in mESC Cultures.** Approximately 1 to 5% mESCs of an ESC population sporadically enter the 2C-like state that express *Zscan4* and *MERVLs* (23–25). Moreover, transient bursts of *Zscan4* expression are accompanied by the rapid derepression of heterochromatin in mouse mESCs (44). This study examined the static heterochromatin state in both fixed Zscan4$^+$ and Zscan4$^-$ cells and observed a decrease in heterochromatin in Zscan4$^+$ cells. We wondered whether there was a direct link of reduced heterochromatic foci with elevated Zscan4 expression levels or vice versa. We generated *Zscan4* promoter-driven Tomato-Red mESCs and performed time-lapse live cell imaging of the Tomato-Red$^+$ mESCs to examine the dynamics of Zscan4 expression. Red fluorescence indicative of Zscan4 and Hoechst 33342-stained heterochromatin was revealed in live cell imaging. Increased intensity of Tomato-Red coincided with fewer and larger Hoechst-stained heterochromatin foci, which eventually lead to diminished heterochromatin foci (Fig. 1 *D*, *Upper*). In contrast, the reduced Tomato-Red fluorescence was associated with an increased number of Hoechst-stained heterochromatin foci and brighter signals (Fig. 1 *D*, *Lower*). Increased Zscan4 expression was accompanied by vigorous heterochromatin remodeling, with initial clusters of heterochromatin followed by rapid decondensation. The heterochromatin foci were reestablished following declined Zscan4 expression (Fig. 1*D*). The Tomato-Red$^+$ cells colocalized with endogenous Zscan4 (green) exhibited fewer but larger heterochromatic foci as indicated by the DAPI staining (Fig. 1 *E* and *F*). A majority of *Zscan4*-driven Tomato-Red$^+$ cells were stained positive for Zscan4 protein (Fig. 1*E*), suggesting that the Tomato-Red signals could indicate the presence of Zscan4 protein in cells. The Tomato protein from the *Zscan4* reporter was present in both the nucleus and cytoplasm, although sometimes the signal in the cytoplasm was too weak to be clearly seen. The live cell imaging experiment suggests that heterochromatin dynamic change is negatively correlated with Zscan4 expression levels.

By comparing the immunofluorescence of Zscan4$^+$ with that of Zscan4$^-$ cells, we observed fewer, but larger heterochromatin foci that coincided with DAPI-densely stained regions in Zscan4$^+$ cells and decreased number of DAPI foci overlapping with increased Zscan4 expression level (Fig. 1 *F* and *G*). It remains unclear whether and how Zscan4 could be involved in heterochromatin organization and decondensation.

To further investigate the heterochromatin dynamics in Zscan4$^+$ cells, we stained H3K9me3 in the *Zscan4* reporter lines and examined the colocalization of H3K9me3 foci with DAPI-dense constitutive heterochromatin foci. H3K9me3 foci in Zscan4$^+$ cells were larger and decondensed, despite fewer than that in Zscan4$^-$ cells (Fig. 1 *H–J*). A similar pattern of heterochromatin distribution as the one observed in Zscan4$^+$ cells was also identified by coimmunofluorescence with heterochromatin protein HP1α (Fig. 1 *K* and *L*). Heterochromatic H3K9me3 and protein HP1α are organized and then disassembled in Zscan4$^+$ cells. Collectively, these results suggest that Zscan4 may mediate heterochromatin remodeling.

**Zscan4 Interacts with the Corepressors and Heterochromatin Modifiers.** Furthermore, we investigated the Zscan4 interactome. Since the early 2C embryos available were insufficient for protein interaction studies, we performed Zscan4 coimmunoprecipitation followed by mass spectrometry (Co-IP/MS) using *Zscan4* overexpression (OE) mESCs (Fig. 2*A*). Co-IP using Zscan4 antibody followed by western blotting confirmed that Zscan4 protein was precipitated, in contrast to the IgG served as negative control (Fig. 2*B*). Similar proteins were identified to interact with

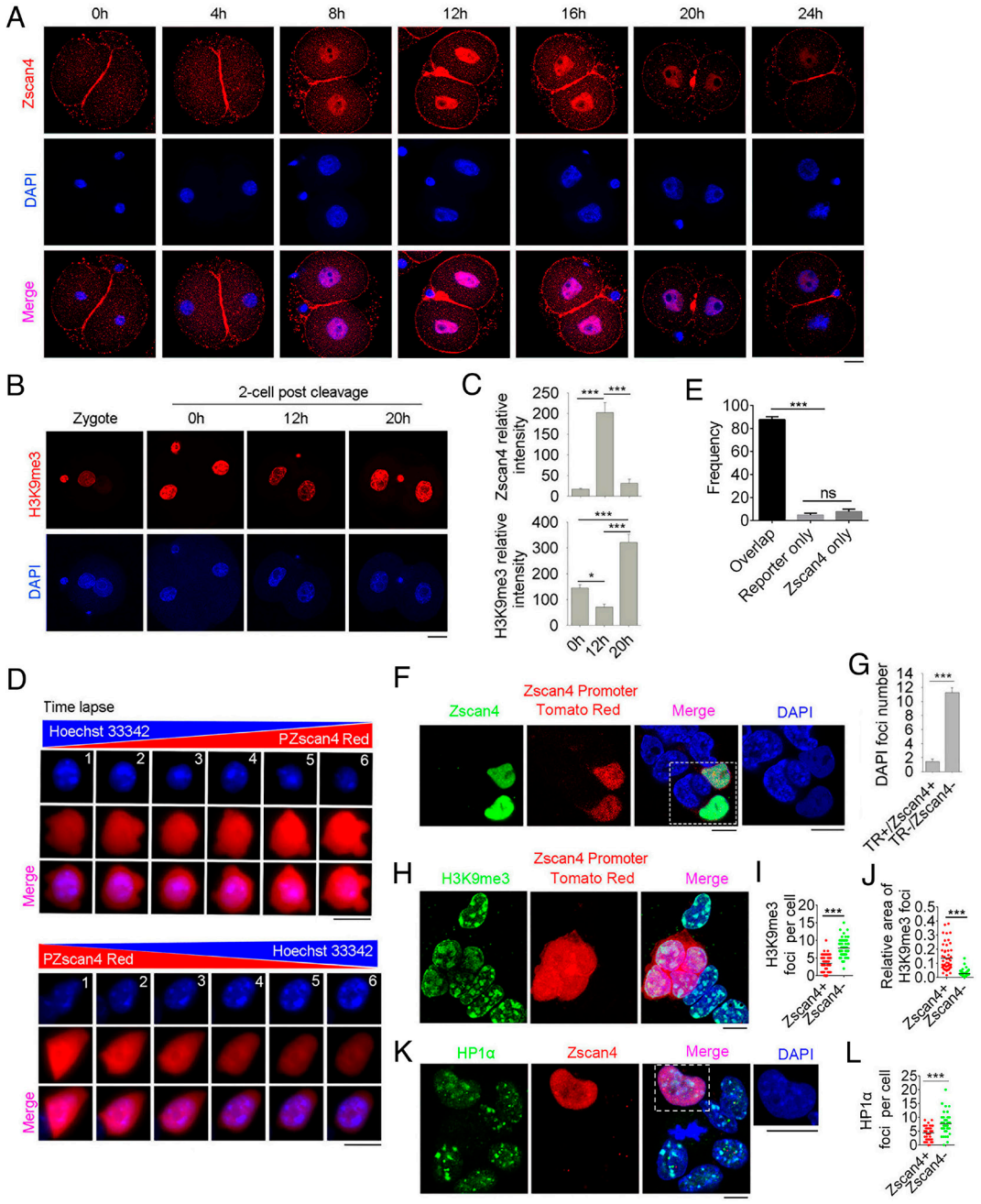


**Fig. 1.** Dynamics of Zscan4 and heterochromatin remodeling in 2C mouse embryos and mESCs. (*A*) Representative images of Zscan4 protein expression by fluorescence microscopy of 2-cell mouse embryos using anti-Zscan4 (red) antibody. DAPI stained nucleus in blue. (Scale bar, 10 μm.) (*B*) H3K9me3 immunofluorescence (red) images of heterochromatin in zygotes and 2C embryos. (Scale bar, 10 μm.) (*C*) Quantification of the relative levels of Zscan4 and H3K9me3 as shown in *B*. Number of 2C embryos analyzed for Zscan4: n ≥ 7; mean ± SEM. *$P < 0.05$ and ***$P < 0.001$. (*D*) Zscan4 dynamics in heterochromatin remodeling. Images captured from live cell imaging microscopy video of *Zscan4* promoter-driven Tomato Red ESCs and Hoechst 33342 revealing distinct dynamics of heterochromatin foci. (*E*) Quantification of the frequency of cells with *Zscan4* reporter positive only (indicative of *Zscan4* promoter activity), Zscan4 protein positive only (indicated by Zscan4 antibody IF), or overlap of each other. n = 49. (*F*) Immunofluorescence microscopy of Zscan4 (Green) with the *Zscan4* promoter-driven Tomato Red (Red). DAPI was used to stain the nucleus (blue). Heterochromatin foci were reduced or disappeared in Zscan4$^+$ cells. (*G*) Quantification of DAPI-dense heterochromatin foci in Tomato Red (TR)$^+$/Zscan4$^+$ and Tomato Red (TR)$^-$/Zscan4$^-$ cells (Zscan4$^+$, n = 26; Zscan4$^-$, n = 29). (*H*) Immunofluorescence of H3K9me3 (green) in Zscan4 promoter-driven Tomato Red mESCs. (*I* and *J*) Quantification of the number of H3K9me3 foci per cell (n = 62) (*I*) and relative average area of H3K9me3 foci (n = 50) between Zscan4$^-$ and Zscan4$^+$ cells (*J*), as shown in *H*. (*K*) Immunofluorescence of HP1α (green) in Zscan4-positive (red) ESCs. (Scale bar, 10 μm.) (*L*) Quantification of the number of HP1α foci per cell between Zscan4$^-$ and Zscan4$^+$ cells, as shown in *K*. ***$P < 0.001$.

Zscan4 in the two independent MS repeats (Dataset S1). Notably, numerous proteins were found to be associated with histone modifications, corepressors, or E3 ligases (Fig. 2*C*). Transient coexpression of Flag-Zscan4 and HA-Kap1/Trim28, -Hdac1 (histone deacetylase1), -Lsd1 (histone demethylase1), -Trim25 (a ubiquitin ligase E3), -Caf1, -Eif3c, -Mta2, -Npm1, -Eif4a3, or -Rnf181, and of Nedd4-Flag indicated that Zscan4 interacts with Kap1/Trim28, Hdac1, Lsd1/Kdm1A, and Trim25 (Fig. 2*D*), while no interactions were detected between Zscan4 and Caf1, Eif4a3, Mta2, Npm1, Eif3c, Rnf181, or Nedd4 (*SI Appendix*, Fig. S2*A*). Previous studies also demonstrated that Zscan4 could interact with Kap1, Hdac1, Lsd1, and Brg1 (44, 45). Zscan4 interacting with Kap1, Hdac1, Lsd1, or H3K9me3 was also observed in mouse ESCs using Zscan4 antibody or Flag-Zscan4 (*SI Appendix*, Fig. S2 *B* and *C*). The Zscan4 interaction network based on MS and Co-IP data is summarized in *SI Appendix*, Fig. S2*D*.

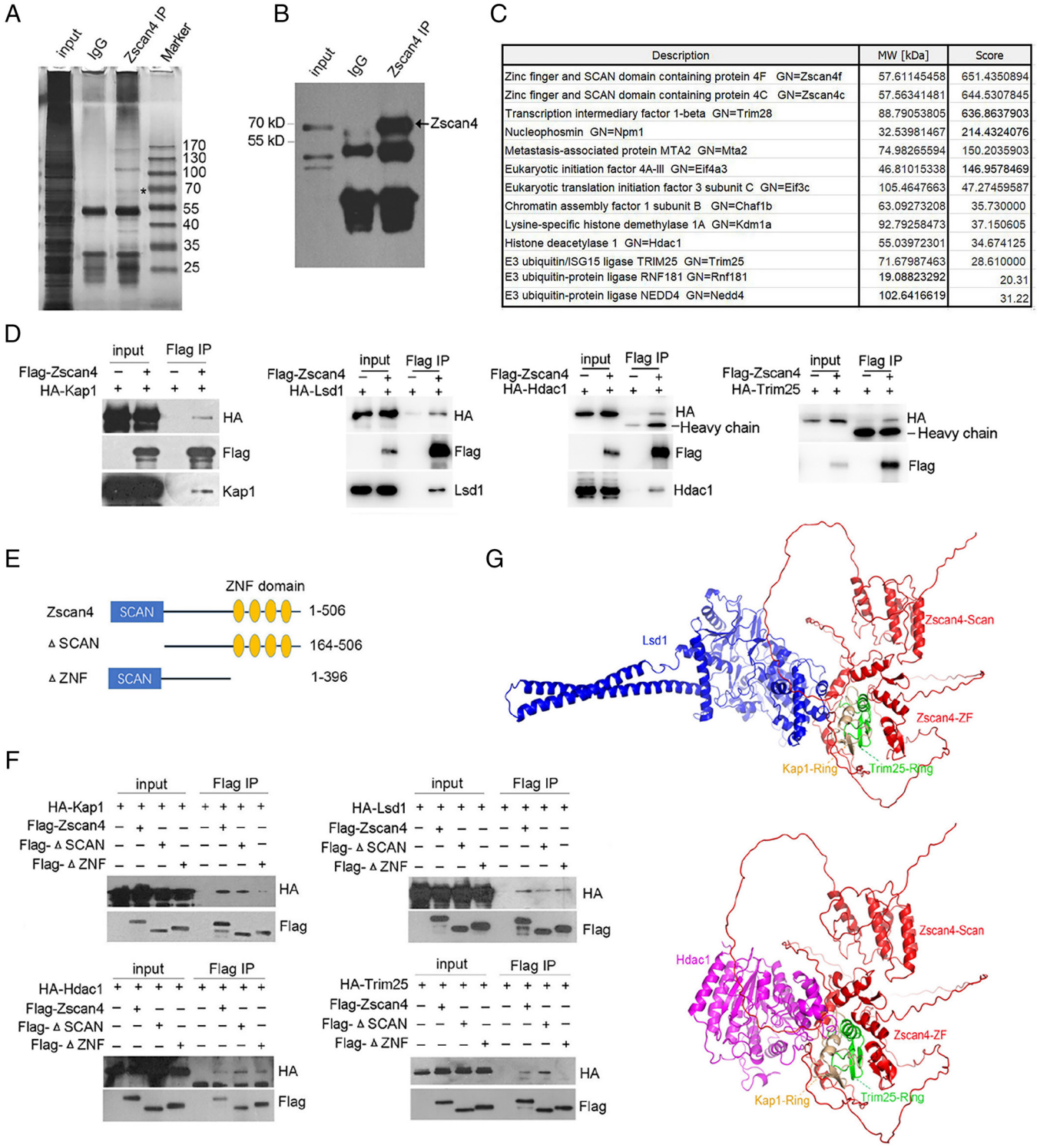


| Description | MW [kDa] | Score |
|---|---|---|
| Zinc finger and SCAN domain containing protein 4F GN=Zscan4f | 57.61145458 | 651.4350894 |
| Zinc finger and SCAN domain containing protein 4C GN=Zscan4c | 57.56341481 | 644.5307845 |
| Transcription intermediary factor 1-beta GN=Trim28 | 88.79053805 | 636.8637903 |
| Nucleophosmin GN=Npm1 | 32.53981467 | 214.4324076 |
| Metastasis-associated protein MTA2 GN=Mta2 | 74.98265594 | 150.2035903 |
| Eukaryotic initiation factor 4A-III GN=Eif4a3 | 46.81015338 | 146.9578469 |
| Eukaryotic translation initiation factor 3 subunit C GN=Eif3c | 105.4647663 | 47.27459587 |
| Chromatin assembly factor 1 subunit B GN=Chaf1b | 63.09273208 | 35.730000 |
| Lysine-specific histone demethylase 1A GN=Kdm1a | 92.79258473 | 37.150605 |
| Histone deacetylase 1 GN=Hdac1 | 55.03972301 | 34.674125 |
| E3 ubiquitin/ISG15 ligase TRIM25 GN=Trim25 | 71.67987463 | 28.610000 |
| E3 ubiquitin-protein ligase RNF181 GN=Rnf181 | 19.08823292 | 20.31 |
| E3 ubiquitin-protein ligase NEDD4 GN=Nedd4 | 102.6416619 | 31.22 |

**Fig. 2.** Identification of Zscan4 interactome and functional domains in interacting with corepressors. (*A*) Silver staining gel image of Zscan4-interacting proteins that were immunoprecipitated from *Zscan4* OE mESCs treated with MG-132 and identified by mass spectrometry. Putative Zscan4 proteins are indicated with an asterisk. (*B*) Western blot of endogenous Zscan4 from IP sample. (*C*) List of representative proteins identified in the Zscan4 Co-IP/MS. Scores of the identified peptide are indicated. (*D*) IP-western blot validation of Co-IP/MASS data for selected proteins. Shown are interacting proteins with Zscan4 such as Kap1, Lsd1, Hdac1, and Trim25. (*E*) Schematic drawings of full-length Zscan4, SCAN domain depleted (ΔSCAN) and zinc finger motifs depleted (ΔZNF) truncated proteins. (*F*) Western blotting of HA-Hdac1, HA-Lsd1, HA-Kap1, and HA-Trim25 proteins following exogenously expressed Flag-Zscan4 (full length), ΔSCAN or ΔZNF and IP (using an anti-Flag antibody) in HEK293T cells. (*G*) Protein–protein interaction docking of the predicted structure of mouse Zscan4c (red) by AlphaFold with the crystal structure of human Hdac1 (magenta), Lsd1 (blue), Kap1-Ring (sand), and Trim25-Ring (green), respectively. (*Upper*) Zscan4c-ZF interacts with the N-terminal SWIRM domain of Lsd1 and may help to recruit Lsd1 to the E3 ligase center of Trim25. (*Bottom*) The ring domain of Kap1, ring domain of E3 ligase Trim25, and full-length Hdac1 interact with adjacent surfaces of the Zinc finger domain of Zscan4c, suggesting that Zscan4c may facilitate recruitment of Hdac1 to the E3 ligase center of Trim25.

Moreover, using Zscan4 mutants by deletion of either the SCAN or the Zinc-Finger (ZNF) domain (Fig. 2*E*), we identified specific domain-partner binding interactions (Fig. 2*F*). The SCAN or ZNF domain deletion mutants interacted with Hdac1 or Lsd1 (Fig. 2*F*), suggesting that the link region (aa 164 to 396) between the two domains likely recruits the repressive proteins. The ZNF-truncated mutation of Zscan4 either reduced the interaction with Kap1 or disrupted the interaction with Trim25 (Fig. 2*F*), suggesting that the ZNF domain is required for Zscan4 to interact with Kap1 or Trim25. Kap1 and Trim25 may competitively bind to the ZNF domain of Zscan4 (Fig. 2*F*). Furthermore, by taking advantage of the computational structural prediction with AlphaFold (46), we achieved structural models of Zscan4 protein domains and their interactions with Lsd1, Hdac1, Kap1, and Trim25 (Fig. 2*G*). The structural models faithfully recapitulate the domains that we probed for interaction of Zscan4 with them by the in vitro Co-IP experiments shown above (Fig. 2 *E* and *F*).

To further quantify protein–protein interactions between Zscan4 and the associated proteins in vivo, we performed proximity ligation assay (PLA) (*SI Appendix*, Fig. S3*A*) (47). Zscan4 or Flag-Zscan4 was shown to interact with Kap1, Lsd1, Hdac1, and H3K9me3 in vivo (*SI Appendix*, Fig. S3*B*). The number of PLA foci may indicate the variations of their interactions (*SI Appendix*, Fig. S3*C*).

Kap1 is a member of a transcriptional corepressor complex and could interact with heterochromatin reader HP1, histone methyltransferase (HMT) Setdb1, as well as histone deacetylation and methylation to establish a de novo niche of heterochromatin (48). We demonstrated that Kap1 could interact with H3K9 HMTs such as Suv39h1, Suv39h2, Setdb1, and G9a (*SI Appendix*, Fig. S4*A*). Zscan4 also interacted with Suv39h1, Suv39h2, Setdb1, and G9a (*SI Appendix*, Fig. S4*B*). Ectopic expression of *Suv39h1* and *Suv39h2* greatly elevated H3K9me3 levels and concomitantly decreased H3K9ac (*SI Appendix*, Fig. S4 *C* and *D*). OE of *G9a* and *Setdb1* had negligible effects on H3K9me3 levels in mESCs (*SI Appendix*, Fig. S4 *C* and *D*), suggesting that H3K9me3 may not be modified by G9a and Setdb1. While Kap1 formed large foci in Zscan4$^+$ cells in most cases, the Kap1 foci were absent in the vast majority of Zscan4$^-$cells and the foci colocalized with heterochromatin foci (*SI Appendix*, Fig. S4*E*), Kap1 formed foci could also colocalize with H3K9me3 specific foci in few cells (*SI Appendix*, Fig. S4*F*). We speculated that Kap1 with formed foci represents Zscan4$^+$ cells, as both Kap1 and H3K9me3 aggregate into large foci in Zscan4$^+$ cells (*SI Appendix*, Fig. S4 *E* and *F*). Suv39h1 was evenly distributed in Zscan4$^+$ cells, which was different from the specific foci in Zscan4$^-$ cells (*SI Appendix*, Fig. S4*G*). G9a protein was distributed in the nucleus and the distribution did not differ between Zscan4$^+$ and Zscan4$^-$ cells (*SI Appendix*, Fig. S4*G*). These data together show that the ZNF domain of Zscan4 interacts with Kap1 and that Kap1 also can interact with Suv39h1 and Suv39h2, involving in heterochromatin assembly.

**Proteasome Degradation of the Corepressors Assembled by Zscan4.** Lsd1 and Hdac1 are core catalytic components of the corepressor complex CoREST, a transcriptional repressor complex, and can maintain repressive or hypoacetylated states of heterochromatin to initiate heterochromatin silencing and propagation (49, 50). Intriguingly, comparison of the fluorescence intensity revealed that Lsd1 and Hdac1 protein levels were significantly lower in Zscan4$^+$ than in Zscan4$^-$ cells (Fig. 3 *A* and *B*). Zscan4$^+$ mESCs sorted by FACS also displayed lower Hdac1 and Lsd1 protein levels compared to Zscan4$^-$ cells by western blot (Fig. 3 *C*, *Left*). Despite significant downregulation of Lsd1 and Hdac1 proteins, their mRNA levels were unaltered in Zscan4$^+$ compared to Zscan4$^-$ cells by analysis of the RNA-seq data (44) (Fig. 3 *C*, *Right*), suggesting posttranscriptional regulation of *Lsd1* and *Hdac1* in Zscan4$^+$ cells. In *Zscan4*-TomatoRed$^+$ cells treated with the proteasome inhibitor MG-132, Lsd1 and Hdac1 protein levels were largely maintained compared to the DMSO treatment control (Fig. 3 *D*–*I*), indicating that they are degraded by the ubiquitin–proteasome system in Zscan4$^+$ cells. To further explore whether the burst expression of *Zscan4* in Zscan4$^+$ cells impairs Lsd1 and Hdac1 protein stability, we modulated *Zscan4* expression in mESCs and assessed the effects on Lsd1 and Hdac1 protein levels. Ectopic transient Zscan4 high expression cells exhibited lower Lsd1 and Hdac1 protein levels (Fig. 3 *J* and *K*). Moreover, Suv39h1 protein level was slightly reduced and protein levels of both Lsd1 and Hdac1 were even further reduced in *Zscan4* stable OE mESCs, whereas Kap1 protein levels remained largely unchanged (Fig. 3*L*). Notably, Lsd1 protein stability is more severely impaired in Zscan4$^+$ and *Zscan4* stable OE cells (Fig. 3 *A*–*C* and *L*). Hence, high expression levels of Zscan4 could lead to reduced levels of Hdac1 and Lsd1 proteins. Together, these results indicate that Zscan4 is responsible for inducing proteasome-mediated Lsd1 and Hdac1 protein degradation in Zscan4$^+$ cells.

We also observed that the highest Zscan4 protein levels during the mid-2C stage (12 h) of mouse embryos coincided with the lowest protein levels of Hdac1 and Lsd1 (*SI Appendix*, Fig. S5*A*). These data suggest that Zscan4 may enable proteasome degradation of Hdac1 and Lsd1 in mouse embryos. Indeed, Hdac1 and Lsd1 underwent polyubiquitinations following addition of Human influenza hemagglutinin (HA)-tagged ubiquitin (*SI Appendix*, Fig. S5*B*). In addition, ubiquitination levels of Hdac1 and Lsd1 were elevated following OE of *Zscan4* in mESCs by Co-IP with the specific antibody (*SI Appendix*, Fig. S5*C*), corroborating their reduced protein levels by western blot (Fig. 3*L*).

Our data show that Hdac1 and Lsd1 proteins are reduced in Zscan4$^+$ cells (Fig. 3 *A*–*C*) and *Zscan4* OE cells (Fig. 3 *J*–*L*). We hypothesized that ectopically expressed *Zscan4* might mediate ubiquitination degradation of Hdac1 and Lsd1. Initially, we compared the OE efficiency of *Zscan4* in mESCs and HEK293T cells. OE efficiency of *Zscan4* in HEK293T cells was higher than that of mESCs (*SI Appendix*, Fig. S5*D*), and only a small proportion of *Zscan4*-overexpressed ESCs can achieve the Zscan4 protein expression level comparable to that of Zscan4$^+$ mESCs (*SI Appendix*, Fig. S5*E*). The Zscan4 protein expression levels as well as the percentage of Zscan4-transiently expressed cells also were higher in 293 T cells following *Zscan4* OE. To enhance the OE effect of *Zscan4*, we utilized HEK293T cells to test whether Zscan4 enables the ubiquitination of the interacting proteins. Indeed, Zscan4 noticeably increased the polyubiquitination levels of Hdac1 and Lsd1, as well as Suv39h1 and Suv39h2, two methyltransferases of H3K9me3 required for constitutive heterochromatin (51) (Fig. 4*A*). Comparatively, Setdb1 and G9a exhibited only minor variation by Zscan4 (Fig. 4*A*). The next question was how Zscan4 mediates the ubiquitination-associated degradation of the corepressors Hdac1 and Lsd1 and heterochromatin modifiers Suv39h1/2.

**Trim25 Is Involved in Zscan4-Mediated Ubiquitination of Lsd1 and Hdac1.** A few E3 ligases were contained in the Zscan4 precipitate following Zscan4 Co-IP/MS (Dataset S1). Further, Co-IP/WB showed that Trim25 interacted with the ZNF domain of Zscan4 (Fig. 2*F*). We knocked out *Trim25* in mESCs by designing gRNA in exon 1 that disrupts the N-terminal E3 ligase-harbored RING domain and confirmed the deficiency of *Trim25* by Sanger sequencing and western blot (Fig. 4 *B* and *C*). Consequently, downregulation of Lsd1 and Hdac1 proteins was largely prevented in Zscan4$^+$ cells in the absence of Trim25 protein (Fig. 4 *D*–*F*), indicating that Trim25 is required for Zscan4-mediated protein degradation of Lsd1 and Hdac1.

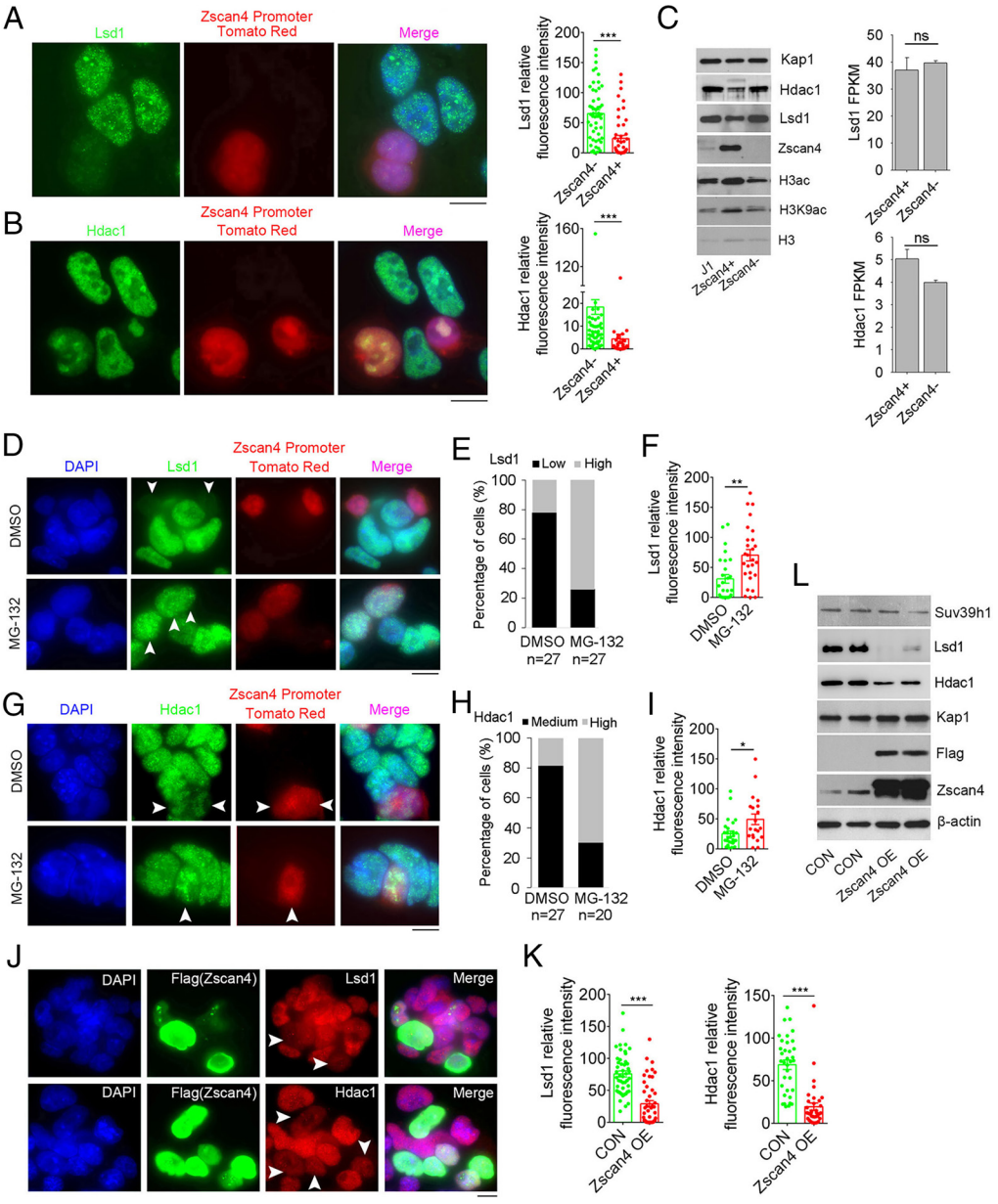


**Fig. 3.** Proteasome degradation of Lsd1 and Hdac1 mediated by Zscan4. (*A*) Immunofluorescence microscopy showing Lsd1 (green) expression in *Zscan4* promoter-driven Tomato Red (Zscan4$^+$) mESCs. DNA was stained with DAPI. (*Right*) Quantitative analysis of the relative fluorescence intensity of Lsd1 in Zscan4$^+$ and Zscan4$^-$ cells (Zscan4$^+$, n = 49; Zscan4$^-$, n = 52). (*B*) Immunofluorescence microscopy showing Hdac1 (green) expression in *Zscan4* promoter-driven Tomato Red (Zscan4$^+$) mESCs. (*Right*) Quantitative analysis of the relative fluorescence intensity of Hdac1 in Zscan4$^+$ and Zscan4$^-$ cells (Zscan4$^+$, n = 64; Zscan4$^-$, n = 64). (*C*) Western blots of Zscan4, Lsd1, Hdac1, Kap1, H3ac, and H3K9ac levels in Zscan4$^+$ cells compared with Zscan4$^-$ cells. (*Right*) mRNA expression level (FPKM) of *Lsd1* and *Hdac1* between Zscan4$^+$ and Zscan4$^-$ cells (44). (*D*) Immunofluorescence of Lsd1 in *Zscan4* promoter-driven tomato Red mESCs between DMSO (Control) and MG-132 (10 μM) treatment for 12 h. Arrows indicate Lsd1 protein levels in Zscan4$^+$ cells. (Scale bar, 10 μm.) (*E*) Quantification of the data in *D*. (*F*) Quantitative analysis of the relative fluorescence intensity of Lsd1 in Zscan4$^+$ cells. (*G*) Immunofluorescence of Hdac1 in *Zscan4* promoter-driven tomato Red mESCs between DMSO (Control) and MG-132 (10 μM) treatment for 12 h. Arrows indicate Hdac1 protein levels in Zscan4+ cells. (*H*) Quantification of the data in *G*. The total number of Zscan4+ cells counted between DMSO and MG132 treatments are indicated, and the results are shown as percentages. When the fluorescence intensity in Zscan4+ cells is similar to or stronger than neighbor Zscan4− cells, those Zscan4+ are referred to Hdac1-high or Lsd1-high groups, otherwise Hdac1-medium or Lsd1-low groups (*E* and *H*). (*I*) Quantitative analysis of the relative fluorescence intensity of Hdac1 in Zscan4+ cells. (*J*) Immunofluorescence of Lsd1 and Hdac1 with Flag (fused with Zscan4) after *Zscan4* transient transfection. Arrows indicate Lsd1 and Hdac1 lower levels in Flag-Zscan4 highly expressed cells. (Scale bar, 10 μm.) (*K*) Quantitative estimate of the relative fluorescence intensity of Lsd1 (n = 47) and Hdac1 (n = 35) between *Zscan4* highly OE and control (CON). (*L*) Western blots of Suv39h1, Lsd1, Hdac1, Kap1, Flag, and Zscan4 in *Zscan4* stable OE compared with control (CON) mESCs. **P* < 0.05, ***P* < 0.01, and ****P* < 0.001.

To test whether Trim25 can directly ubiquitinate Lsd1 and Hdac1, we performed an in vitro ubiquitination assay using purified proteins. Trim25 could robustly ubiquitinate Lsd1 and Hdac1 (Fig. 4 *G–I*). Zscan4 also was ubiquitinated by Trim25 (Fig. 4 *G Left*, 4th lane). Unexpectedly, Zscan4 is not necessary to promote Trim25-dependent ubiquitination of Hdac1 in vitro (Fig. 4*G*). This may be explained by that for in vitro ubiquitination experiment, the components are simple and close, and the protein concentration is high, such that Trim25 alone can accomplish the role of ubiquitination of the target substrates. In contrast, Trim25 alone may not efficiently target and ubiquitinate the repressors in vivo, but requires Zscan4 acting as an adaptor to promote this event. Additional E3 ligases that remained to be identified might also be involved in the ubiquitination of Lsd1 and Hdac1 in the repressive histone complex.

**Trim25 and Kap1/Trim28 Competitively Bind to Zscan4.** Kap1 captured in Zscan4 Co-IP/MS is a RING-type E3 ubiquitin transferase besides acting as a corepressor. To assess the potential role of Kap1 as an E3 ligase for ubiquitination of Hdac1 and Lsd1, we showed that Kap1 interacts with Hdac1 and Lsd1 (Fig. 5*A*). Yet, Kap1 could not increase ubiquitination levels of Hdac1 and Lsd1 in vivo (Fig. 5*B*) and in vitro (Fig. 5*C*). These data indicated that Kap1 is not an E3 ligase for ubiquitination of Hdac1 and Lsd1. Intriguingly, the presence of Kap1 notably reduced the ability of Trim25 in ubiquitinating Hdac1 and Lsd1 proteins (Fig. 5*C*). Hence, Kap1 and Trim25 are mutually exclusive despite they both can bind to the ZNF domain of Zscan4 as predicted by the above structural modeling (Fig. 2 *F* and *G*).

Given that Kap1 appeared to inhibit or interfere with Hdac1 and Lsd1 ubiquitination by Trim25 (Fig. 5*C*), we assumed that Kap1 would be degraded or released from Zscan4 in the presence of Trim25. We performed IP/western blot experiments and demonstrated that Kap1 do not interact with Trim25 (Fig. 5*D*). However, Kap1-Flag (5th band) pulled down by HA (Zscan4) was stronger than the Flag band in the presence of Trim25 (6th band) (Fig. 5*E*), indicating that Kap1 and Trim25 compete for binding to the ZNF domain of Zscan4. Yet, *Trim25* OE did not reduce Kap1 protein levels (Fig. 5*F*). These data together suggest

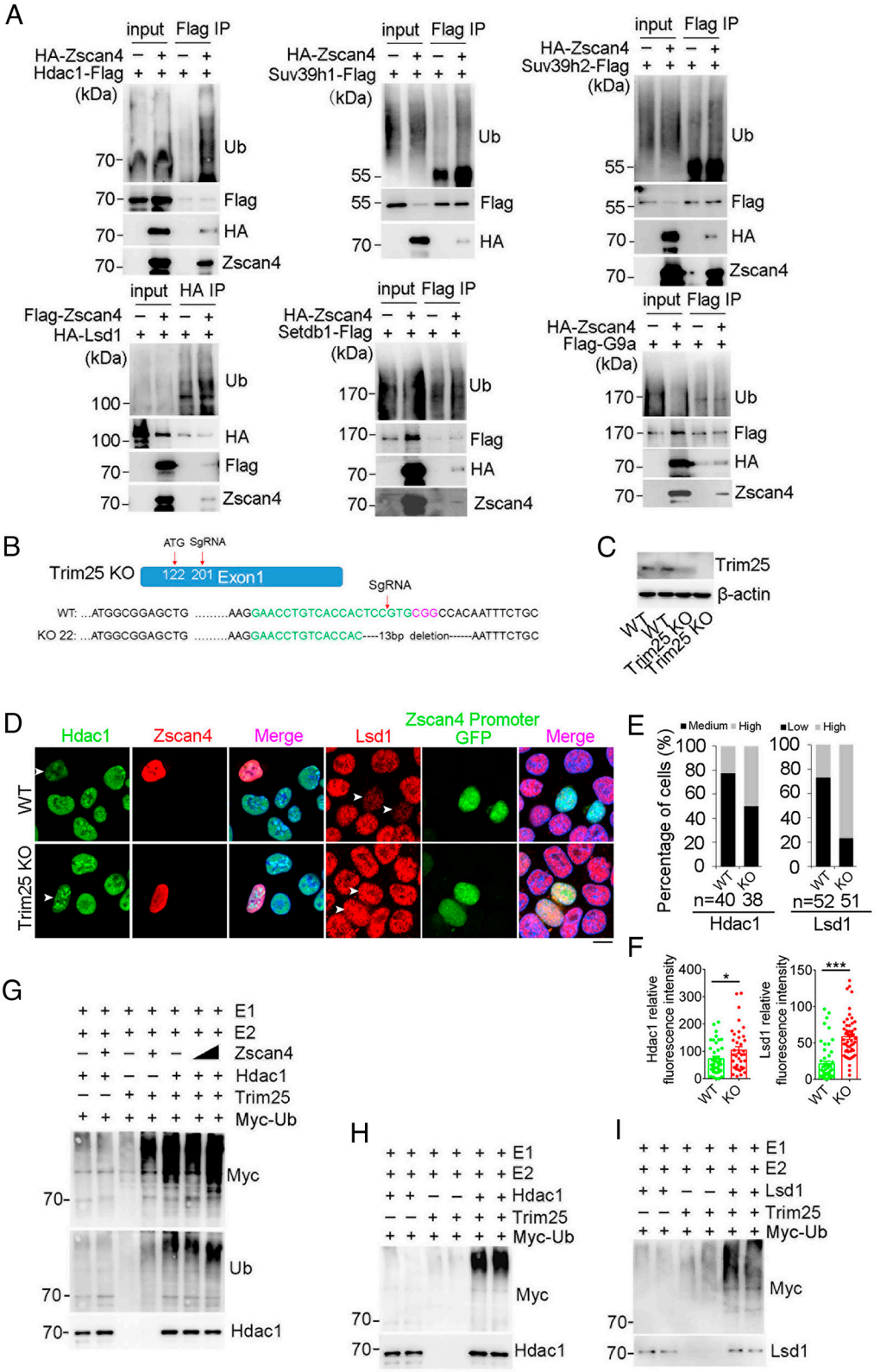


**Fig. 4.** Zscan4 mediates polyubiquitination-induced degradation of the interacting proteins via Trim25. (*A*) Ubiquitination of Hdac1, Lsd1, Suv39h1, or Suv39h2, but not of Setdb1 and G9a following OE of *Zscan4* in HEK293T cells. n ≥ 3 repeats. (*B*) Schematic representation of *Trim25* knockout (KO) using CRISPR/Cas9 and Sanger sequencing of WT as well as *Trim25*-KO cell lines. The gRNA sequence locates in Exon 1, and *Trim25*-KO clone #22 displays 13 bp sequence deletion in both alleles, which results in the disruption of E3 ligase RING domain and frameshift. (*C*) Western blotting confirmation of *Trim25*-KO mESC lines with Trim25 antibody. (*D*) Immunofluorescence microscopy of Lsd1 and Hdac1 in WT and *Trim25*-KO mESCs. Arrows indicate Hdac1 and Lsd1 immunofluorescence in Zscan4$^+$ cells. Since both Lsd1 and Zscan4 antibodies are rabbit polyclonal, *Zscan4c* promoter-driven AcGFP1 expression reporter plasmid was first transfected into WT and *Trim25*-KO mESCs to indicate Zscan4$^+$ cells. (*E*) Quantitative estimate of fluorescence intensity of Lsd1 and Hdac1 in Zscan4$^+$ cells between WT and *Trim25*-KO mESCs. The total number of Zscan4$^+$ cells counted between WT and *Trim25*-KO mESCs are indicated, and the results are shown as percentages. (*F*) Quantitative analysis of the relative fluorescence intensity of Lsd1 and Hdac1 in Zscan4$^+$ cells between WT and *Trim25*-KO mESCs. (*G–I*) In vitro ubiquitination assay using purified proteins of Trim25 to ubiquitinate Hdac1 in the presence of Zscan4 (*G*) or absence of Zscan4 (*H*) and Lsd1 in the absence of Zscan4 (*I*). Each experiment contained two biological repeats. $^*P < 0.05$, $^{**}P < 0.01$, and $^{***}P < 0.001$.

that Trim25 may block binding of Kap1 to Zscan4, allowing itself to access and ubiquitinate Hdac1 and Lsd1.

**Zscan4 Is Linked to Heterochromatin Disassembly and Elevated Histone Acetylation.** Elevated Zscan4 reduced Lsd1 and Hdac1, in association with notable reduction of heterochromatin foci revealed by DAPI staining (Fig. 3 *J* and *K*). Heterochromatic foci as indicated by H3K9me3 as well as by DAPI staining were reduced in the cells with the highest Zscan4 protein expression levels in *Zscan4* OE mESCs, while the H3K9me3 foci, which were colocalized with DAPI-stained heterochromatin foci, appeared to assemble around the Zscan4 protein clusters in cells with increasing levels of Zscan4 (*SI Appendix*, Fig. S6*A*). Kap1 foci formation also could be seen with increased expression of Zscan4 (*SI Appendix*, Fig. S6*B*), also supporting the notion that Kap1 is involved in Zscan4

interaction with chromatin repressors and heterochromatin modifiers.

Moreover, we examined the functions of specific Zscan4 domains in remodeling heterochromatin using the constructed mutants (Fig. 2*E*). H3K9me3 lost clustering and aggregation functions after ZNF deletion but not after SCAN deletion of Zscan4 (*SI Appendix*, Fig. S6*C*). While H3K9me3 foci aggregated into cluster in *Zscan4*-OE cells when Zscan4 was intact or mutated (ΔSCAN), H3K9me3 foci remained when Zscan4 was mutated (ΔZNF). We estimated that the frequency of H3K9me3 aggregation is decreased after deleting the ZNF domain of Zscan4 (*SI Appendix*, Fig. S6*C*). Loss of heterochromatin aggregation or foci could be observed in WT ESCs or mESCs with SCAN mutated domain, whereas the typical foci remained in the ZNF mutated mESCs. These data show that the ZNF domain of Zscan4 contributes to heterochromatin assembly and remodeling.

Furthermore, we assessed whether histone acetylation is increased in Zscan4$^+$ mESCs. Higher levels of H3 acetylation including H3K9ac and H3K27ac (Fig. 3*C* and *SI Appendix*, Fig. S6 *D*–*F*) were observed in Zscan4$^+$ cells. Additionally, H3K9ac and H3K27ac formed large foci in Zscan4$^+$ cells (*SI Appendix*, Fig. S6 *E* and *F*). Thus, reduced heterochromatin foci or disassembly of heterochromatin is accompanied by accumulation of H3 acetylation, H3K9ac and H3K27ac in Zscan4$^+$ cells. On the contrary, OE of *Suv39h1* or *Suv39h2* elevated H3K9me3 and reduced H3K9ac levels (*SI Appendix*, Fig. S4*C*). We also examined histone acetylation levels in 2C embryos. Levels of H3K9ac and H3K27ac were noticeably increased at 12 and 20 h post cleavage in 2C embryos (*SI Appendix*, Fig. S6 *G* and *H*). Zscan4 induction also increased levels of H3K27ac in cancer cells (52). Elevated levels of H3K9ac and H3K27ac in Zscan4$^+$ cells in an mESC population and the dynamic changes of Zscan4, H3K9ac, and H3K27ac in 2C embryos link Zscan4 to the elevated histone acetylation.

**Zscan4 Promotes Chromatin Accessibility to Activate the 2C State.** To test whether elevated Zscan4 indeed can promote the chromatin accessibility and 2C-like gene expression, we performed RNA-seq and Assay for Transposase-Accessible Chromatin using sequencing (ATAC-seq) analysis of *Zscan4* OE mESCs compared to that of control mESCs. It appeared that 2,765 genes were up-regulated and 2,617 genes were down-regulated in *Zscan4* OE mESCs (adjusted $P < 0.05$, fold change ≥2). The 1,053 representative 2C-specific genes were chosen in our RNA-seq and ATAC-seq analyses, based on a previous report on the identification of representative 2C genes by scRNA-seq analysis (53). Representative 2C-like genes, such as *Zscan4, Usp17l, Pramel7, Zfp560, Dppa4, Dppa2*, and *Tbx3* were up-regulated in *Zscan4* OE mESCs (Fig. 6*A*). More retrotransposons including *L1Md* and *MERVL*, typical 2C markers, were also up-regulated following OE of *Zscan4* (Fig. 6*B*). In agreement, Zscan4 activates *MERVL* and cleavage embryo genes (54). These data further substantiate the notion that Zscan4 can modulate 2C-like genes and transposable elements (TEs) in mESCs.

Moreover, ATAC-seq revealed that elevated Zscan4 leads to increased chromatin accessibility compared to that of the controls. The promoters at genome-wide levels were more open following *Zscan4* OE (Fig. 6*C*). *Zscan4* OE increased ATAC-seq signals at promoters of up-regulated 2C-like genes (Fig. 6*D*) and also of up-regulated *MERVL-int* (Fig. 6*E*), which is consist with the overall increase in chromatin accessibility across the genome. This increase was particularly pronounced at promoters of up-regulated genes and *MERVL* elements (*MT2_Mm* and *MERVL-int*) in MERVL$^+$Zscan4$^+$ cells (19). Moreover, more open chromatin was found near *MERVL* at the early 2C stage, when *Zscan4* is actively transcribed (10). The *Z*-score of 2C-like gene expression [Transcripts Per Million (TPM)] following *Zscan4* OE was associated with ATAC-seq enrichment (Reads Per Kilobase per Million mapped reads) (Fig. 6*F*). For instance, *1600002K03Rik*, *2310011J03Rik*, *Pramel6/7*, *Zfp935*, and *Zfp809* up-regulated following *Zscan4* OE coincided with elevated ATAC enrichment at their promoters bound by H3K4me3 and H3K27ac (*SI Appendix*, Fig. S7).

Next, we attempted to look at whether Zscan4, Lsd1, Hdac1, and Kap1 can bind to the same regions of 2C-like genes and retrotransposons by taking advantage of the valuable data available from public database reported in mESCs. Combining analysis of reported Zscan4 ChIP-seq (29), with those of Lsd1 (55), Hdac1 (56), Kap1 (57), and H3K9me3 (58), demonstrated that Zscan4, Lsd1, Hdac1, and Kap1 bind to the same regions of 2C-like genes activated in *Zscan4* OE mESCs (Fig. 6*G*), with much less H3K9me3 enrichment (Fig. 6*G*). Moreover, both Zscan4 and H3K9me3 turned out to bind to the similar sites of 2C-like retrotransposons up-regulated in *Zscan4* OE mESCs cells, including *L1Md* in *Line1* family and *MERVL*, coincided with the abundance

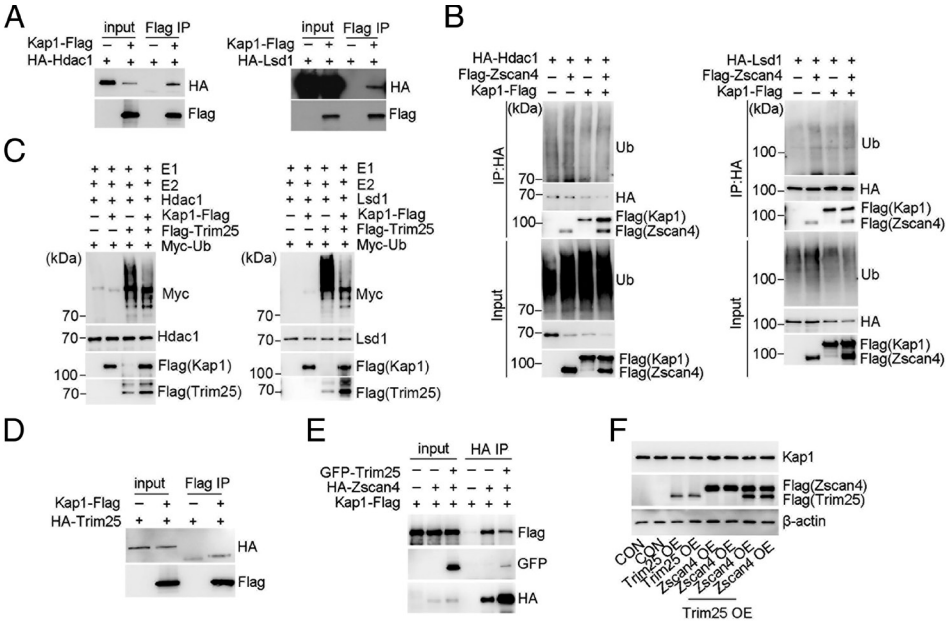


**Fig. 5.** Trim25 releases Kap1 from binding to Zscan4. (*A*) IP/western blot of Kap1 interactions with Hdac1 and Lsd1 in HEK293T cells. (*B*) Ubiquitination of Hdac1 and Lsd1 following OE of *Zscan4* and *Kap1* in HEK293T cells. (*C*) In vitro ubiquitination assay using purified proteins demonstrating that Trim25 but not Kap1 can ubiquitinate Hdac1 and Lsd1. The presence of Kap1 decreases Trim25 ubiquitination activity of Hdac1 or Lsd1. (*D*) IP/western blot showing that Kap1 does not interact with Trim25 in HEK293T cells. (*E*) IP/western blot of HA (Zscan4) interaction with Flag (Kap1) in the presence or absence of Trim25. (*F*) Western blotting of Kap1 and Flag in *Trim25* OE in control and *Zscan4* OE mESC lines. Each experiment contained two biological repeats.

of Lsd1, Hdac1, and Kap1 at these sites (Fig. 6*H*). Together, the specific enrichment of Zscan4 and corepressors at 2C-like genes and retrotransposons likely explain their increased chromatin accessibility and upregulation in *Zscan4* OE mESCs.

H3K4me3 represents an active chromatin marker. Using the H3K4me3 ChIP-seq data publicly available (59), we showed that H3K4me3 level is elevated on 2C-like genes such as *Bad*, *Tbx3*, *1600002K03Rik*, *Usp17le*, *Zscan4c*, *Zfp352*, *Zfp935*, and *Zfp809* in Zscan4$^+$ cells, compared with that of mESCs (*SI Appendix*, Fig. S8*A*). Dux has been shown to activate *Zscan4* and to be both necessary and sufficient to convert mESCs into 2CLCs (20). We detected that *Dux* expression is up-regulated in *Zscan4* OE cells (*SI Appendix*, Fig. S8*B*). *Zscan4* OE resulted in a significant upregulation of *Dux* transcript, and OE of *Dux* also induced *Zscan4* expression (34). *Dux* is expressed in mouse embryos before ZGA-defining genes and necessary for formation of 2CLCs (20, 31), suggesting that positive feedback loops act to reinforce the 2C-like state. A small number of Dux (20) binding sites on the genome overlap with Zscan4 binding sites (*SI Appendix*, Fig. S8*C*), including some Zscan4-activated 2C-like genes (*SI Appendix*, Fig. S8*D*). Dux and Zscan4 bind to the same regions of the 2C-like genes including *Zscan4c* and *Zfp352*, or *L1* and *MERVL* (*SI Appendix*, Fig. S8*E*). These results suggest that Dux and Zscan4 play a coordinated role in 2CLCs. These and the above results together indicate that Zscan4-mediated ubiquitination and degradation of chromatin repressors Lsd1 and Hdac1 promotes chromatin accessibility of 2C-like genes and retrotransposons.

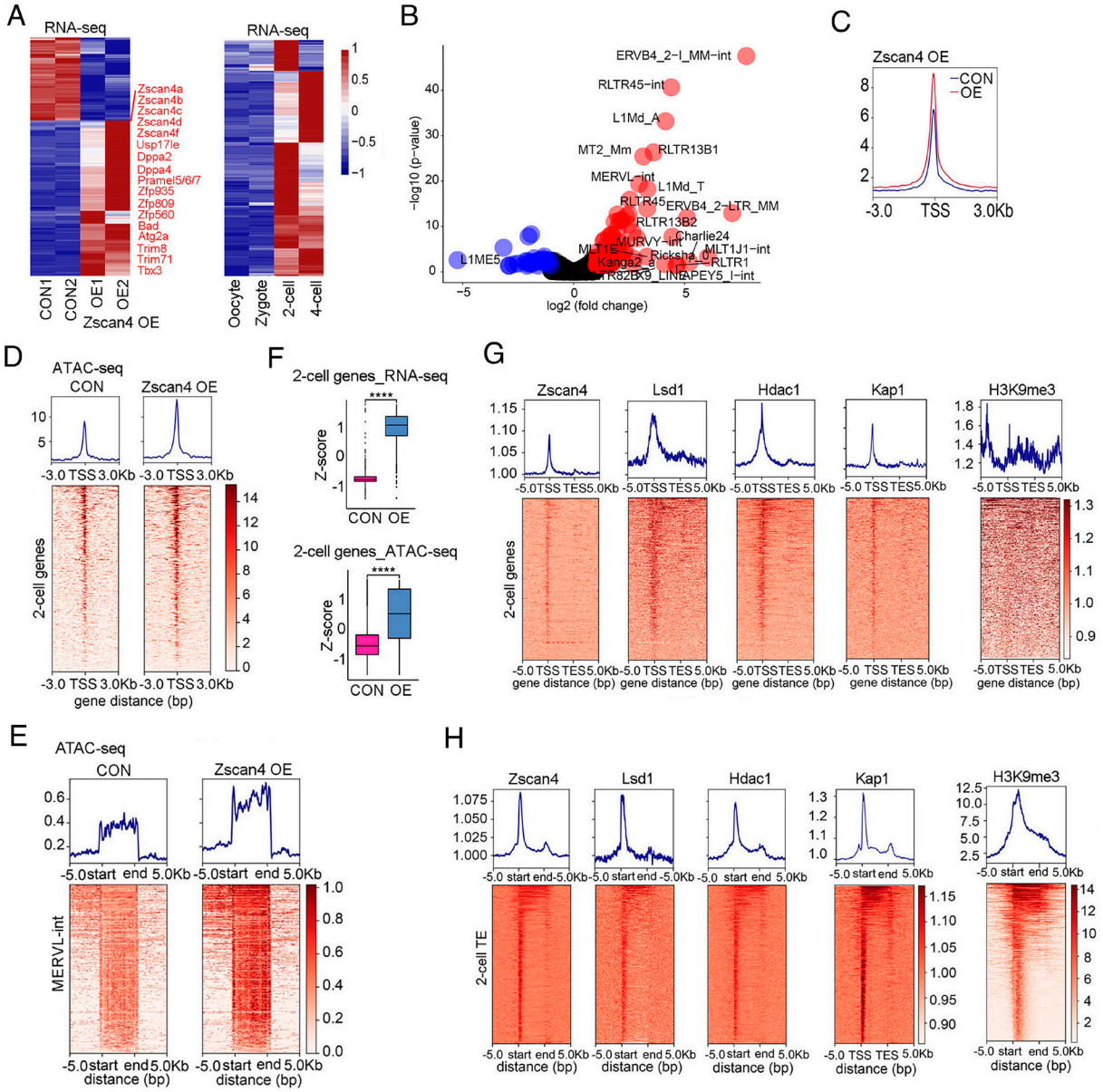


**Fig. 6.** Zscan4 promotes chromatin accessibility and up-regulates 2C-like genes and retrotransposons in ESCs. (*A*) Heatmap showing expression of representative 2C-like genes according to single-cell RNA-seq in preimplantation embryos data (53). The genes including the Zscan4 family up-regulated are marked in red on the *Right*. (*B*) Scatter diagrams of TEs expression after *Zscan4* OE. (*C*) The average profile showing the ATAC-seq signals in *Zscan4* OE mESCs compared with WT control (CON). (*D*) The average profile and heatmap of the ATAC-seq enrichment around accessible promoters at 2C-like genes up-regulated after *Zscan4* OE from *A*. (*E*) The average profile and heatmap of the ATAC-seq enrichment at the start and end sites of *MERVL-int* up-regulated in *Zscan4* OE mESCs. (*F*) Z-score of 2C-like gene expression (TPM) and ATAC-seq enrichment after *Zscan4* OE. (*G* and *H*) Plot of Zscan4, Lsd1, Hdac1, Kap1, and H3K9me3 binding profile and heatmap at TSS and TES of 2C-like genes (*G*) and retrotransposons (*H*) up-regulated in *Zscan4* OE mESCs. The ChIP-seq signals are calculated as the ratio of normalized reads relative to input. TES, transcription end site. Data from GSE140621 (29) (Zscan4 ChIP-seq data from Zscan4$^+$ cells), GSE18515 (55) (Lsd1 ChIP-seq), GSE183292 (56) (Hdac1 ChIP-seq), GSE70799 (57) (Kap1 ChIP-seq), or GSE98256 (58) (H3K9me3 ChIP-seq).

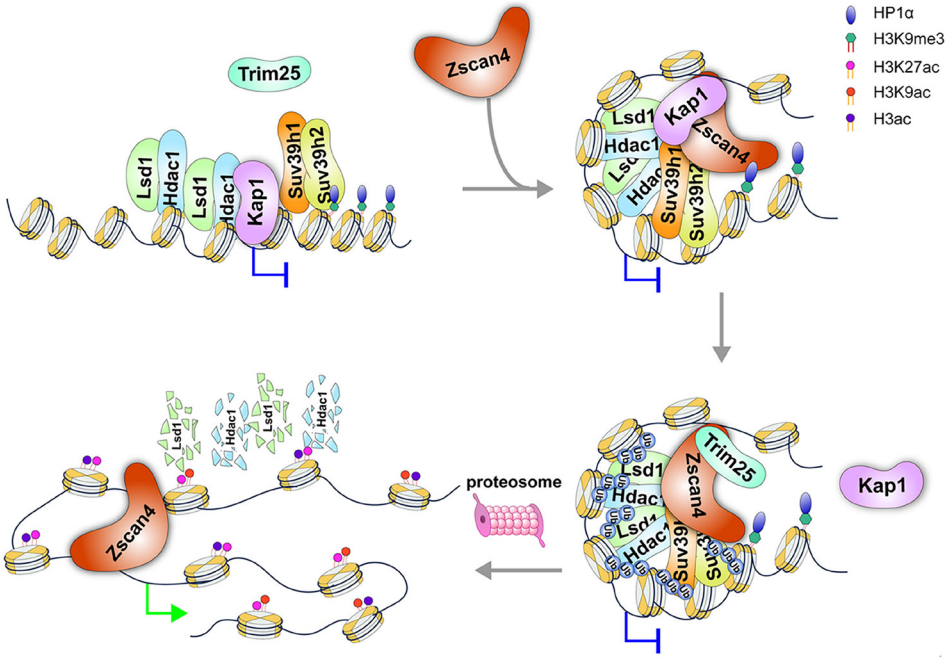


**Fig. 7.** Proposed simplified model for Zscan4 function in chromatin remodeling. During the accumulation of Zscan4 protein, Zscan4 interacts with Kap1, Hdac1, and Lsd1 and with heterochromatin modifiers such as Suv39h1 and Suv39h2, transiently forming a large repressive chromatin complex (specific foci can be observed under the microscopy). The E3 ligase Trim25 is then recruited to Zscan4 through the ZNF domain, to release Kap1 from Zscan4, allowing polyubiquitination and degradation of the corepressors such as Hdac1 and Lsd1 mediated by Trim25. Decompaction of repressive chromatin promotes histone acetylation and increases chromatin accessibility for promoting the 2C-like state.

## Discussion

We propose a simplified model to illustrate the mechanism by which Zscan4 mediates chromatin remodeling in 2CLCs (Fig. 7). When Zscan4 begins to express and gradually accumulates, it interacts with the corepressor complex including Kap1, Hdac1, and Lsd1, and also with heterochromatin modifiers such as Suv39h1/2, transiently forming a large repressive chromatin complex (specific foci can be observed under the microscopy). Indeed, elevating expression of Zscan4 is often accompanied by accumulated foci of Kap1 (*SI Appendix*, Fig. S4*E*), also with the specific H3K9me3 foci (*SI Appendix*, Fig. S4*F*). Hence, Kap1 is initially involved in Zscan4 interacting with the chromatin repressors. The E3 ligase Trim25 is then recruited to Zscan4 through the ZNF domain to release Kap1 from Zscan4, allowing polyubiquitination and degradation of the corepressors such as Hdac1 and Lsd1 mediated by Trim25. Degradation and disassembly of the repressive chromatin complex results in increased histone acetylation and chromatin accessibility for promoting the 2C-like state (Fig. 7).

In 2C embryos, the highest Zscan4 protein levels 12 h post zygotic cleavage also coincide with decreased Lsd1 and Hdac1levels (*SI Appendix*, Fig. S5*A*). These data together with the above proteasome experiments suggest that only sufficient levels of Zscan4 protein can lead to proteasome degradation of the corepressors Lsd1 and Hdac1. We detected the role of Trim25 activity in the ubiquitination of repressive protein complexes in mESCs. Actually, mouse early embryos also express Trim25 protein increased from zygote to 2C stage, identified by quantitative mass spectrometry (60). Further experiments are required to validate Trim25's role in cleavage embryos, even though it is quite challenging to prove it directly due to the scarcity of 2C-embryos. We also do not exclude the possibility that additional E3 ligases may cooperate with Trim25 for effective ubiquitination of the corepressors and histone modifiers.

An intermediate population characterized by its *Zscan4* expression was identified as a precursor of 2CLCs in ESC cultures and PRC1 components as inhibitors of the 2C-like state (61). Furthermore, ATAC-seq analysis demonstrates that 2CLCs have an open chromatin structure at *MERVL* sites, and *Zscan4* activation precedes chromatin opening at *MERVL* sites (19, 61). Additionally, other epigenetic modifiers such as PRC1.6, EP400–TIP60 (61), DOT1L, and KDM5B (40), might function together in 2CLC emergence. While increased global chromatin accessibility facilitates the activation of 2C genes and retrotransposons, burst expression of retrotransposons such as *Line-1* can contribute to chromatin opening (12). Chromatin accessibility and retrotransposon activation might act as positive feedback to ensure the full activation of 2C genes.

Moreover, one family of genome activators known as the DUX transcription factors (DUX in the mouse and DUX4 in the human) activate hundreds of ZGA genes, including endogenous retroviral elements, such as *MERVL* in mice and *HERVL* in humans (20, 31, 32). DUX has been shown to activate *Zscan4* and to be both necessary and sufficient to convert mESCs into 2CLCs (20). Transcription of minor ZGA (such as *Zscan4*) and major ZGA is regulated by Pol II in a step-wise manner and is associated with chromatin opening (14). Furthermore, minor ZGA is repressed by cohesin, and increased H3K27ac derepresses minor ZGA gene promoters (62). Histone acetylation promotes chromatin accessibility and correlates with active transcription in vivo (63). Increased chromatin accessibility promoted by Zscan4 presumably creates the conditions necessary for transcription factors to recruit Pol II to major ZGA sites (14). It is likely that the transcription factors function sequentially and in concert with Zscan4 and Pol II to fully activate ZGA.

Zscan4 forms a repressive complex with Lsd1 and Hdac1 and recruits E3 ligase such as Trim25 to promote ubiquitination for degradation of Lsd1 and Hdac1. The 2C-like genes silenced by corepressors are then derepressed and activated by elevated histone acetylation. Kap1 acts as a scaffold for a silencing complex that comprises Hdac1 and Lsd1, in repression of sequences derived from TEs (64, 65). Moreover, Kap1, Hdac1, and Lsd1 in the corepressor complex can constitute with H3K9me3 in the heterochromatin (48, 66). Kap1 and H3K9me3 deposited by Setdb1 and Suv39h1/2 repress retrotransposons such as *Line-1* and *ERVs* (66, 67). The selective enrichment of Zscan4 with the corepressors Lsd1, Hdac1, and Kap1 at 2C-like genes and retrotransposons likely explains their increased accessibility and specific elevation after ubiquitination and degradation of Lsd1 and Hdac1 by Trim25, in *Zscan4* OE mESCs (Fig. 6 *G* and *H*). Zscan4 binding to the active enhancers further promotes transcription of 2C genes and retrotransposons including *MERVL* (54). Taken together, our data extend previous findings and reveal molecular

insights into the mechanisms whereby Zscan4 mediates ubiquitination and degradation of repressive chromatin complex and thus promotes chromatin accessibility to fully activate the 2C-like state in mESCs.

2CLCs mimic 2C embryos to large extent in terms of many molecular, epigenetic, and metabolic features, such as burst expression of ZGA genes and retrotransposons, global DNA demethylation, high chromatin accessibility, loss of chromocenters and disruption of nucleoli, slow DNA replication fork speed, decreased glycolytic and respiratory activity and increased glucose uptake (68). The identification of 2CLCs in mESCs provides a surrogate in vitro model for 2C embryos and has greatly extended our understanding toward totipotency and early embryonic development (69). Nevertheless, 2CLCs are not equivalent to the 2C embryos in the natural ZGA process. The natural ZGA process in mice includes the transcription of both the paternal and maternal genomes. The first wave of transcription (also referred to as minor ZGA) starts at the mid-one-cell stage shortly after pronuclear formation and largely comes from the paternal genome (70), probably due to the rapid active DNA demethylation of the male pronucleus in the one-cell stage by the DNA dioxygenase Tet3 (71, 72). The minor ZGA is promiscuous with low-level and genome-wide transcription (73), serving as a prerequisite for major ZGA. In contrast, the emergence of 2CLC occurs in a relatively uniform diploid chromatin of mESCs. Moreover, 2CLCs only activate a subset of mouse ZGA genes in 2C embryos (24). Thus, the findings based on 2CLCs might not recapitulate that in natural 2C embryos and should be validated cautiously. For instance, contrary to the key function of Dux in inducing the 2C-like state in mESCs, loss of *Dux* causes only minor defects in ZGA and is compatible with mouse development (74–76). Therefore, future work will be needed to confirm whether Zscan4 is also responsible for the ubiquitination and degradation of corepressors and increased chromatin accessibility of 2C genes in 2C embryos during the natural ZGA process.

## Materials and Methods

**Animals and ES Cells.** Use of mice for this research was approved by the Institutional Animal Care and Use Committee at Nankai University. Mice used in this study were taken care of and operated according to the relevant regulations and housed in individually ventilated cages on a standard 12 h light: 12 h dark cycle in the sterile Animal Facility.

J1 mESCs, E14 mESCs, *Zscan4* OE mESCs, *Zscan4* promoter-driven Tomato-red protein expression mESCs, HeLa, and HEK293T were used. J1 ESCs and E14 mESCs were cultured without feeder. The ES cell culture medium consisted of knock-out Dulbecco's Modified Eagle's Medium (DMEM) (Gibco) with 15% fetal bovine serum (FBS, ES quality HyClone), 1,000 U/mL mouse leukemia inhibitory factor (ESGRO, Chemicon), 0.1 mM nonessential amino acids, 0.1 mM β-mercaptoethanol, 1 mM L-glutamine, and penicillin (100 U/mL) and streptomycin (100 μg/mL) (77). The medium was changed daily, and cells were routinely passaged every 2 d. HeLa and HEK293T cells were grown in DMEM (Invitrogen) supplemented with 10% FBS (HyClone), 1 mM L-glutamine (Invitrogen), 100 U/mL penicillin (Invitrogen), and 100 mg/mL streptomycin (Invitrogen).

**Vector Construction.** Murine *Zscan4c* coding sequences (CDS) was cloned into pCMV-Tag 2B, Pb-3×Flag vector. Murine, (*Kap1*, *Hdac1*, *Nedd4, Suv39h1*, *Suv39h2*, *Setdb1,* and *G9a* CDS were cloned into GFP-3×flag vector (gift from Lingyi Chen lab, State Key Laboratory of Medicinal Chemical Biology, Nankai University, Tianjin 300350, China) or Pb-3×Flag vector. Stable cell lines were established from single clone after 7 to 10 d in G-418 for pCMV-Tag2B, hygro for pb-3× Flag, or puromycin selection for OE-3×flag. Murine *Zscan4*, *Mta2*, *Npm1*, *Caf1*, *Eif3c*, *Eif4a3*, *Kap1*, *Lsd1*, *Hdac1, Rnf181,* and *Trim25* CDS were cloned into pCMV-HA vector.

**Co-IP.** Cells were cotransfected with epitope-tagged expression plasmids. 48 h after transfection, cells were harvested with 500 μL lysis buffer (20 mM Tris-HCL PH 8.0, 100 mM NaCl, 0.5% NP-40, 1 mM EDTA) supplemented with protease inhibitor cocktail (#04693132001, Roche) and PMSF (#PB0425). The cell lysate was rotated at 4 °C for 30 min. After centrifugation at 13,000 g for 10 min, the supernatants were used for IP. The cell extracts were incubated with anti-Flag antibody (F1804 Sigma) overnight at 4 °C, followed by incubation with lysis buffer and washed in 50 μL of Protein G Sepharose™ 4 Fast Flow (17-0618-01 GE Healthcare) for 3 h. The incubated Protein G was washed with lysis buffer at 4 °C for 10 min. The cell extracts (input 50 μL) and IP samples were then subjected to western blot with anti-Flag (F1804 Sigma) or anti-HA (KM8004) antibodies for detecting protein–protein interactions. Zscan4 antibody (AB4340 Millipore) was used for IP. Other primary antibodies included Kap1 (ab22553, Abcam), Lsd1 (ab17721, Abcam), Hdac1 (06-720, Upstate), or H3K9me3 (ab8898, Abcam).

**Mass Spectrometry.** Due to unstable nature of the Zscan4 protein based on our initial observations, MG-132 (a potent, reversible and cell-permeable proteasome inhibitor) was added to potentially reduce degradation of Zscan4 protein in *Zscan4* OE ESCs. For mass spectrometry analysis of the endogenous murine Zscan4 and its associated proteins, the immunoprecipitate was run on the 10% Bis-Tris sodium dodecyl sulfate-polyacrylamide gel electrophoresis and separated 2 cm from the well (Coomassie blue without running to the separating gel). The gel was cut and used for mass spectrometry analysis by PTM BIO Company (Hangzhou). The experiments were independently repeated twice and consistent results obtained.

**Statistical Analysis.** Statistics were analyzed by using the StatView software from Statistical Analysis Systems Institute Inc. (Cary, NC). Data were analyzed using two-tailed unpaired Student's *t* test to compare two groups or ANOVA to compare more than two groups and expressed as mean ± SEM. *P* values less than 0.05 were considered significant ($*P < 0.05$, $**P < 0.01$, or $***P < 0.001$). Graphs were generated using GraphPad Prism or R package ggplot2 or other R packages described in the method details.

**Data, Materials, and Software Availability.** The accession number for all the RNA sequencing data reported in this paper is NCBI GEO: GSE141489, and the ATAC sequencing data in this paper are NCBI GEO: GSE141490. Published data analyzed are available in Gene Expression Omnibus under accession GSE140621 (Zscan4 ChIP-seq data from Zscan4$^+$ cells) (29), GSE18515 (Lsd1) (55), GSE183292 (Hdac1) (56), GSE70799 (Kap1) (57), GSE72784 (H3K4me3) (78), GSE38596 (H3K27ac) (79), GSE125238 (H3K27ac) (35), GSE98256 (H3K9me3 ChIP-seq) (58), GSE85632 (Dux ChIP-seq) (20), or GSE164486 (H3K4me3 ChIP-seq) (59). All data are included in the manuscript and/or supporting information.

**ACKNOWLEDGMENTS.** We thank Lingyi Chen for providing OE-3×flag vector, Cheng Yang for Duolink PLA kit, Haifeng Fu and Peng Gong for assisting the experiments, Yuequan Shen, Yanjun Li, and Guo Chen for discussing experiments, and Yifei Liu, Renjing Liu, Zhucheng Chen, and Falong Lu for critical reading and comments on revising the manuscript. This study was supported by China National Key R&D Program (2018YFA0107000), National Natural Science Foundation of China (32030033, 82230052 and 32270845), Haihe Laboratory of Cell Ecosystem Innovation Fund, and Tianjin Science and/or Technology Plan Key Project (20JCZDJC00550).

Author affiliations: [a]State Key Laboratory of Medicinal Chemical Biology, Nankai University, Tianjin 300350, China; [b]Department of Cell Biology and Genetics, Frontiers Science Center for Cell Responses, Nankai University, Tianjin 300350, China; [c]State Key Laboratory of Primate Biomedical Research, Institute of Primate Translational Medicine, Kunming University of Science and Technology, Kunming, Yunnan 650500, China; [d]Yunnan Key Laboratory of Primate Biomedical Research, Kunming, Yunnan 650500, China; [e]Haihe Laboratory of Cell Ecosystem, Chinese Academy of Medical Sciences & Peking Union Medical College, Tianjin 300020, China; [f]Department of Biochemistry and Molecular Biology, College of Life Sciences, Nankai University, Tianjin 300071, China; [g]College of Pharmacy, Nankai University, Tianjin 300350, China; [h]Department of Cell Biology, School of Basic Medical Sciences, Tianjin Medical University, Tianjin 300070, China; and [i]Institute of Translational Medicine, Tianjin Union Medical Center, Nankai University, Tianjin 300000, China

1. A. Burton, M. E. Torres-Padilla, Chromatin dynamics in the regulation of cell fate allocation during early embryogenesis. *Nat. Rev. Mol. Cell Biol.* **15**, 723–734 (2014).
2. M. T. Lee, A. R. Bonneau, A. J. Giraldez, Zygotic genome activation during the maternal-to-zygotic transition. *Annu. Rev. Cell Dev. Biol.* **30**, 581–613 (2014).
3. J. Rossant, Genetic control of early cell lineages in the mammalian embryo. *Annu. Rev. Genet.* **52**, 185–201 (2018).
4. M. A. Eckersley-Maslin, C. Alda-Catalinas, W. Reik, Dynamics of the epigenetic landscape during the maternal-to-zygotic transition. *Nat. Rev. Mol. Cell Biol.* **19**, 436–450 (2018).
5. K. N. Schulz, M. M. Harrison, Mechanisms regulating zygotic genome activation. *Nat. Rev. Genet.* **20**, 221–234 (2019).
6. Z. Zou *et al.*, Translatome and transcriptome co-profiling reveals a role of TPRXs in human zygotic genome activation. *Science* **378**, abo7923 (2022).
7. S. Ji *et al.*, OBOX regulates mouse zygotic genome activation and early development. *Nature* **620**, 1047–1053 (2023).
8. X. Liu *et al.*, Distinct features of H3K4me3 and H3K27me3 chromatin domains in pre-implantation embryos. *Nature* **537**, 558–562 (2016).
9. F. Lu *et al.*, Establishing chromatin regulatory landscape during mouse preimplantation development. *Cell* **165**, 1375–1388 (2016).
10. J. Wu *et al.*, The landscape of accessible chromatin in mammalian preimplantation embryos. *Nature* **534**, 652–657 (2016).
11. I. M. Flyamer *et al.*, Single-nucleus Hi-C reveals unique chromatin reorganization at oocyte-to-zygote transition. *Nature* **544**, 110–114 (2017).
12. J. W. Jachowicz *et al.*, LINE-1 activation after fertilization regulates global chromatin accessibility in the early mouse embryo. *Nat. Genet.* **49**, 1502–1510 (2017).
13. C. Wang *et al.*, Reprogramming of H3K9me3-dependent heterochromatin during mammalian embryo development. *Nat. Cell Biol.* **20**, 620–631 (2018).
14. B. Liu *et al.*, The landscape of RNA Pol II binding reveals a stepwise transition during ZGA. *Nature* **587**, 139–144 (2020).
15. K. Zhang *et al.*, Analysis of genome architecture during SCNT reveals a role of cohesin in impeding minor ZGA. *Mol. Cell* **79**, 234–250.e9 (2020).
16. A. V. Probst, F. Santos, W. Reik, G. Almouzni, W. Dean, Structural differences in centromeric heterochromatin are spatially reconciled on fertilisation in the mouse zygote. *Chromosoma* **116**, 403–415 (2007).
17. A. Sankar *et al.*, KDM4A regulates the maternal-to-zygotic transition by protecting broad H3K4me3 domains from H3K9me3 invasion in oocytes. *Nat. Cell Biol.* **22**, 380–388 (2020).
18. B. Zhang *et al.*, Allelic reprogramming of the histone modification H3K4me3 in early mammalian development. *Nature* **537**, 553–557 (2016).
19. M. A. Eckersley-Maslin *et al.*, MERVL/Zscan4 network activation results in transient genome-wide DNA demethylation of mESCs. *Cell Rep.* **17**, 179–192 (2016).
20. P. G. Hendrickson *et al.*, Conserved roles of mouse DUX and human DUX4 in activating cleavage-stage genes and MERVL/HERVL retrotransposons. *Nat. Genet.* **49**, 925–934 (2017).
21. T. Ishiuchi *et al.*, Early embryonic-like cells are induced by downregulating replication-dependent chromatin assembly. *Nat. Struct. Mol. Biol.* **22**, 662–671 (2015).
22. A. Boskovic *et al.*, Higher chromatin mobility supports totipotency and precedes pluripotency in vivo. *Genes Dev.* **28**, 1042–1057 (2014).
23. M. Zalzman *et al.*, Zscan4 regulates telomere elongation and genomic stability in ES cells. *Nature* **464**, 858–863 (2010).
24. T. S. Macfarlan *et al.*, Embryonic stem cell potency fluctuates with endogenous retrovirus activity. *Nature* **487**, 57–63 (2012).
25. Q. Deng, D. Ramskold, B. Reinius, R. Sandberg, Single-cell RNA-seq reveals dynamic, random monoallelic gene expression in mammalian cells. *Science* **343**, 193–196 (2014).
26. M. Markiewicz-Potoczny *et al.*, TRF2-mediated telomere protection is dispensable in pluripotent stem cells. *Nature* **589**, 110–115 (2021).
27. J. Dan *et al.*, Zscan4 inhibits maintenance DNA methylation to facilitate telomere elongation in mouse embryonic stem cells. *Cell Rep.* **20**, 1936–1949 (2017).
28. L. Liu *et al.*, Telomere lengthening early in development. *Nat. Cell Biol.* **9**, 1436–1441 (2007).
29. R. Srinivasan *et al.*, Zscan4 binds nucleosomal microsatellite DNA and protects mouse two-cell embryos from DNA damage. *Sci. Adv.* **6**, eaaz9115 (2020).
30. J. Jiang *et al.*, Zscan4 promotes genomic stability during reprogramming and dramatically improves the quality of iPS cells as demonstrated by tetraploid complementation. *Cell Res.* **23**, 92–106 (2013).
31. A. De Iaco *et al.*, DUX-family transcription factors regulate zygotic genome activation in placental mammals. *Nat. Genet.* **49**, 941–945 (2017).
32. J. L. Whiddon, A. T. Langford, C. J. Wong, J. W. Zhong, S. J. Tapscott, Conservation and innovation in the DUX4-family gene network. *Nat. Genet.* **49**, 935–940 (2017).
33. A. De Iaco, A. Coudray, J. Duc, D. Trono, DPPA2 and DPPA4 are necessary to establish a 2C-like state in mouse embryonic stem cells. *EMBO Rep.* **20**, e47382 (2019).
34. M. Eckersley-Maslin *et al.*, Dppa2 and Dppa4 directly regulate the Dux-driven zygotic transcriptional program. *Genes Dev.* **33**, 194–208 (2019).
35. Y. L. Yan *et al.*, DPPA2/4 and SUMO E3 ligase PIAS4 opposingly regulate zygotic transcriptional program. *PLoS Biol.* **17**, e3000324 (2019).
36. R. Le *et al.*, Dcaf11 activates Zscan4-mediated alternative telomere lengthening in early embryos and embryonic stem cells. *Cell Stem Cell* **28**, 732–747.e9 (2021).
37. A. Iturbide *et al.*, Retinoic acid signaling is critical during the totipotency window in early mammalian development. *Nat. Struct. Mol. Biol.* **28**, 521–532 (2021).
38. H. Shen *et al.*, Mouse totipotent stem cells captured and maintained through spliceosomal repression. *Cell* **184**, 2843–2859.e20 (2021).
39. Y. Xu *et al.*, Derivation of totipotent-like stem cells with blastocyst-like structure forming potential. *Cell Res.* **32**, 513–529 (2022).
40. M. Yang *et al.*, Chemical-induced chromatin remodeling reprograms mouse ESCs to totipotent-like stem cells. *Cell Stem Cell* **29**, 400–418.e13 (2022).
41. Y. Hu *et al.*, Induction of mouse totipotent stem cells by a defined chemical cocktail. *Nature* **617**, 792–797 (2023).
42. P. Du, J. Wu, Hallmarks of totipotent and pluripotent stem cell states. *Cell Stem Cell* **31**, 312–333 (2024).
43. G. Falco *et al.*, Zscan4: A novel gene expressed exclusively in late 2-cell embryos and embryonic stem cells. *Dev. Biol.* **307**, 539–550 (2007).
44. T. Akiyama *et al.*, Transient bursts of Zscan4 expression are accompanied by the rapid derepression of heterochromatin in mouse embryonic stem cells. *DNA Res.* **22**, 307–318 (2015).
45. K. I. Ishiguro *et al.*, Expression analysis of the endogenous Zscan4 locus and its coding proteins in mouse ES cells and preimplantation embryos. *In Vitro Cell. Dev. Biol. Anim.* **53**, 179–190 (2017).
46. J. Jumper *et al.*, Highly accurate protein structure prediction with AlphaFold. *Nature* **596**, 583–589 (2021).
47. O. Soderberg *et al.*, Direct observation of individual endogenous protein complexes in situ by proximity ligation. *Nat. Methods* **3**, 995–1000 (2006).
48. J. Padeken, S. P. Methot, S. M. Gasser, Establishment of H3K9-methylated heterochromatin and its functions in tissue differentiation and maintenance. *Nat. Rev. Mol. Cell Biol.* **23**, 623–640 (2022).
49. G. P. Vicent *et al.*, Unliganded progesterone receptor-mediated targeting of an RNA-containing repressive complex silences a subset of hormone-inducible genes. *Genes Dev.* **27**, 1179–1197 (2013).
50. S. Jamaladdin *et al.*, Histone deacetylase (HDAC) 1 and 2 are essential for accurate cell division and the pluripotency of embryonic stem cells. *Proc. Natl. Acad. Sci. U.S.A.* **111**, 9840–9845 (2014).
51. A. H. Peters *et al.*, Histone H3 lysine 9 methylation is an epigenetic imprint of facultative heterochromatin. *Nat. Genet.* **30**, 77–80 (2002).
52. B. A. Portney *et al.*, ZSCAN4 facilitates chromatin remodeling and promotes the cancer stem cell phenotype. *Oncogene* **39**, 4970–4982 (2020).
53. X. Fan *et al.*, Single-cell RNA-seq transcriptome analysis of linear and circular RNAs in mouse preimplantation embryos. *Genome Biol.* **16**, 148 (2015).
54. W. Zhang *et al.*, Zscan4c activates endogenous retrovirus MERVL and cleavage embryo genes. *Nucleic Acids Res.* **47**, 8485–8501 (2019).
55. V. D. Nair *et al.*, Involvement of histone demethylase LSD1 in short-time-scale gene expression changes during cell cycle progression in embryonic stem cells. *Mol. Cell Biol.* **32**, 4861–4876 (2012).
56. W. Mu *et al.*, RBBP4 dysfunction reshapes the genomic landscape of H3K27 methylation and acetylation and disrupts gene expression. *G3 (Bethesda)* **12**, jkac08 (2022).
57. B. X. Yang *et al.*, Systematic identification of factors for provirus silencing in embryonic stem cells. *Cell* **163**, 230–247 (2015).
58. P. Li *et al.*, Rif1 promotes a repressive chromatin state to safeguard against endogenous retrovirus activation. *Nucleic Acids Res.* **45**, 12723–12738 (2017).
59. Y. Zhang *et al.*, Unique patterns of H3K4me3 and H3K27me3 in 2-cell-like embryonic stem cells. *Stem Cell Rep.* **16**, 458–469 (2021).
60. Y. Gao *et al.*, Protein expression landscape of mouse embryos during pre-implantation development. *Cell Rep.* **21**, 3957–3969 (2017).
61. D. Rodriguez-Terrones *et al.*, A molecular roadmap for the emergence of early-embryonic-like cells in culture. *Nat. Genet.* **50**, 106–119 (2018).
62. Z. Du *et al.*, Polycomb group proteins regulate chromatin architecture in mouse oocytes and early embryos. *Mol. Cell* **77**, 825–839.e7 (2020).
63. S. M. Gorisch, M. Wachsmuth, K. F. Toth, P. Lichter, K. Rippe, Histone acetylation increases chromatin accessibility. *J. Cell Sci.* **118**, 5825–5834 (2005).
64. G. Ecco, M. Imbeault, D. Trono, KRAB zinc finger proteins. *Development* **144**, 2719–2729 (2017).
65. A. Laugesen, K. Helin, Chromatin repressive complexes in stem cells, development, and cancer. *Cell Stem Cell* **14**, 735–751 (2014).
66. H. M. Rowe *et al.*, KAP1 controls endogenous retroviruses in embryonic stem cells. *Nature* **463**, 237–240 (2010).
67. N. Liu *et al.*, Selective silencing of euchromatic L1s revealed by genome-wide screens for L1 regulators. *Nature* **553**, 228–232 (2018).
68. H. Xu, H. Liang, The regulation of totipotency transcription: Perspective from in vitro and in vivo totipotency. *Front. Cell Dev. Biol.* **10**, 1024093 (2022).
69. V. Malik, J. Wang, Pursuing totipotency: Authentic totipotent stem cells in culture. *Trends Genet.* **38**, 632–636 (2022).
70. F. Aoki, D. M. Worrad, R. M. Schultz, Regulation of transcriptional activity during the first and second cell cycles in the preimplantation mouse embryo. *Dev. Biol.* **181**, 296–307 (1997).
71. T. P. Gu *et al.*, The role of Tet3 DNA dioxygenase in epigenetic reprogramming by oocytes. *Nature* **477**, 606–611 (2011).
72. T. Nakamura *et al.*, PGC7 binds histone H3K9me2 to protect against conversion of 5mC to 5hmC in early embryos. *Nature* **486**, 415–419 (2012).
73. K. Abe *et al.*, The first murine zygotic transcription is promiscuous and uncoupled from splicing and 3′ processing. *EMBO J.* **34**, 1523–1537 (2015).
74. Z. Chen, Y. Zhang, Loss of DUX causes minor defects in zygotic genome activation and is compatible with mouse development. *Nat. Genet.* **51**, 947–951 (2019).
75. A. De Iaco, S. Verp, S. Offner, D. Grun, D. Trono, DUX is a non-essential synchronizer of zygotic genome activation. *Development* **147**, dev177725 (2020).
76. M. Guo *et al.*, Precise temporal regulation of Dux is important for embryo development. *Cell Res.* **29**, 956–959 (2019).
77. R. Guo *et al.*, Feeders facilitate telomere maintenance and chromosomal stability of embryonic stem cells. *Nat. Commun.* **9**, 2620 (2018).
78. J. A. Dahl *et al.*, Broad histone H3K4me3 domains in mouse oocytes modulate maternal-to-zygotic transition. *Nature* **537**, 548–552 (2016).
79. P. Yu *et al.*, Spatiotemporal clustering of the epigenome reveals rules of dynamic gene regulation. *Genome Res.* **23**, 352–379 (2013).